Available online at www.sciencedirect.com
ScienceDirect
Geochimica et Cosmochimica Acta 72 (2008) 298–310
Geochimica et Cosmochimica Acta
www.elsevier.com/locate/gca

Surface complexation of U(VI) on goethite (α-FeOOH)

David M. Sherman *, Caroline L. Peacock, Christopher G. Hubbard

University of Bristol, Department of Earth Sciences, Bristol BS8 1RJ, UK

Received 19 June 2006; accepted in revised form 17 October 2007; available online 6 November 2007

Abstract

Sorption of U(VI) to goethite is a fundamental control on the mobility of uranium in soil and groundwater. Here, we investigated the sorption of U on goethite using EXAFS spectroscopy, batch sorption experiments and DFT calculations of the energetics and structures of possible surface complexes. Based on EXAFS spectra, it has previously been proposed that U(VI), as the uranyl cation UO_2^{2+}, sorbs to Fe oxide hydroxide phases by forming a bidentate edge-sharing (E2) surface complex, $>Fe(OH)_2UO_2(H_2O)_n$. Here, we argue that this complex alone cannot account for the sorption capacity of goethite (α-FeOOH). Moreover, we show that all of the EXAFS signal attributed to the E2 complex can be accounted for by multiple scattering. We propose that the dominant surface complex in CO_2-free systems is a bidentate corner-sharing (C2) complex, $(>FeOH)_2UO_2(H_2O)_3$ which can form on the dominant {101} surface. However, in the presence of CO_2, we find an enhancement of UO_2 sorption at low pH and attribute this to a $(>FeO)CO_2UO_2$ ternary complex. With increasing pH, U(VI) desorbs by the formation of aqueous carbonate and hydroxyl complexes. However, this desorption is preceded by the formation of a second ternary surface complex $(>FeOH)_2UO_2CO_3$. The three proposed surface complexes, $(>FeOH)_2UO_2(H_2O)_3$, $>FeOCO_2UO_2$, and $(>FeOH)_2UO_2CO_3$ are consistent with EXAFS spectra. Using these complexes, we developed a surface complexation model for U on goethite with a 1-p*K* model for surface protonation, an extended Stern model for surface electrostatics and inclusion of all known UO_2–OH–CO_3 aqueous complexes in the current thermodynamic database. The model gives an excellent fit to our sorption experiments done in both ambient and reduced CO_2 environments at surface loadings of 0.02–2.0 wt% U.

1. INTRODUCTION

Under oxic conditions, uranium is highly soluble due to the formation of a numerous U(VI) complexes in aqueous solutions. The aqueous concentration of U(VI) is limited by its tendency to strongly sorb to Fe oxides and oxide hydroxides (Payne et al., 1994; Waite et al., 1994). In addition to retarding the transport of U in contaminated soil and groundwater, sorption reactions also affect the formation of sediment-hosted U deposits. For example, U(VI) is trapped in the oxidised sandstone above the redox front in the Osamu Utsumi uranium deposit in Brazil (Read, 1992; Waber et al., 1992) and in the Nopal I deposit in Mexico (Prikryl et al., 1997). Sorption of U(VI) by iron (hydr)oxides also retards its mobility during the oxidative weathering of ore deposits (Murakami et al., 1997; von Gunten et al., 1999; Allard et al., 1999). In recent years, concern has emerged about the fate of depleted uranium munitions in soil. Corrosion of such munitions yields schoepite which dissolves to yield UO_2^{2+} in the soil solution. Sorption of U(VI) by iron (hydr)oxide minerals is potentially a significant barrier to contamination of crops and groundwater.

Because of the fundamental importance of iron oxides to the aqueous geochemistry of uranium, a number of studies have been done to understand the mechanisms of U sorption and to develop a surface complexation model that can be used to predict U transport in the soil and groundwater. Hsi and Langmuir (1985) measured sorption of U to goethite (α-FeOOH) and modelled the experiments using monodentate UO_2OH^+ and monodentate, bidentate or tridentate $(UO_2)_3(OH)_5^+$ inner-sphere complexes with a 2-p*K*

* Corresponding author.
E-mail address: dave.sherman@bris.ac.uk (D.M. Sherman).

0016-7037/$ - see front matter © 2007 Elsevier Ltd. All rights reserved.
doi:10.1016/j.gca.2007.10.023

formalism for surface protonation and a triple-layer model for electrostatics. Missana et al. (2003) showed that U sorption to goethite in CO_2-free environments could be modelled using both monodentate and binuclear bidentate complexes in 2-p*K* formalism with, and without, a diffuse-layer model for electrostatics.

Ambiguity about the nature of the UO_2^{2+} surface complex might be overcome with spectroscopy. Waite et al. (1994) used EXAFS spectroscopy to identify the surface complexes of U(VI) on ferrihydrite. At low pH, U binds to ferrihydrite as the hydrated uranyl ion $(UO_2)(H_2O)_n^{2+}$. An inner-sphere surface complex is indicated by a U–Fe distance near 3.5 Å; this distance was taken to indicate a bidentate complex formed by polyhedral edge-sharing by the hydrated uranyl ion, $(UO_2)(H_2O)_n^{2+}$, and a single FeO_6 surface site, $(>Fe–O_2)UO_2(H_2O, OH)_n$. A similar distance was also found by Reich et al. (1998). Here, we shall designate the bidentate edge-sharing complex as E2.

Based on the identified mononuclear bidentate (E2) complex, Waite et al. (1994) modelled their sorption experiments in a 2-p*K* formalism for surface protonation and a diffuse-layer model for electrostatics. They proposed that the surface complexation was much simpler than that proposed by Hsi and Langmuir (1985) and that the complex speciation found in the aqueous phase is not present on the mineral surface. Although their interpretation of the EXAFS was able to resolve only one kind of surface complex (bidentate edge-sharing complex, E2), they needed two different surface sites (''strong and weak sites'') to model their sorption data.

Using EXAFS, Moyes et al. (2000) characterised a surface complex of U on goethite and obtained results similar to those of Waite et al. (1994) for ferrihydrite. However, the E2 complex cannot account for the sorption capacity of goethite for U(VI): goethite forms elongated needles dominated by the {101} surface (e.g., Schwertmann and Murad, 1983; Randall et al., 1999; Boily et al., 2001). Sites that can accommodate the E2 complex are only found on the {210} and {010} surfaces (Fig. 1) and these surfaces comprise only a small fraction of the surface sites on goethite. We hypothesize that there must be an additional surface complex. By analogy with other systems, we hypothesize that there should be a bidentate corner-sharing (designated C2) complex $(>FeOH)_2UO_2$ that can form on the dominant {101} surfaces (Fig. 1). EXAFS spectra of uranium on ferrihydrite (Ulrich et al., 2006) and hematite (Bargar et al., 1999) show evidence for a U–C scattering indicating the presence of UO_2CO_3 ternary complexes. The nature and significance of these complexes on goethite is unclear. We hypothesise that there are several possible ternary complexes on goethite such as $>FeOCO_2UO_2$ or $(>FeOH)_2UO_2CO_3$.

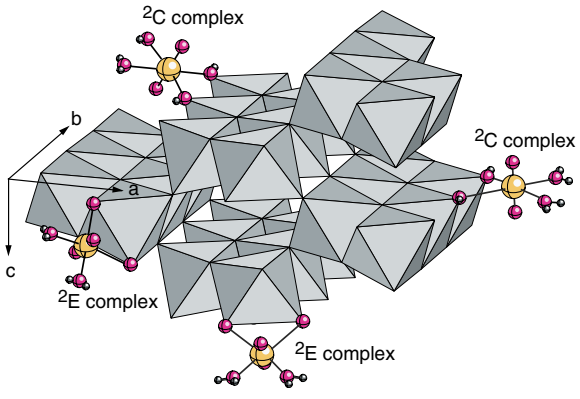

Fig. 1. Hypothetical edge- and corner-sharing U(VI) surface complexes on goethite. Note that in this paper, we are using the standard space group setting Pnma.

In the work described here, we use EXAFS spectroscopy and first-principles calculations to refine these proposed complexes. We present batch sorption experiments are as a function of pH, surface loading and $P(CO_2)$ and develop a surface complexation model that is consistent with our molecular characterization.

2. EXPERIMENTAL AND COMPUTATIONAL METHODS

2.1. Mineral preparation and characterisation

Goethite was prepared by hydrolysis of a $Fe(NO_3)_3$ solution at pH 12–13 and 70 °C for 60 h (Schwertmann and Cornell, 1991). Mineral identity and purity was confirmed by X-ray powder diffraction (XRD) analysis of randomly orientated powder samples. The surface area of the synthesised goethite was measured by BET to be 45 ± 3 m^2/g.

2.2. Potentiometric titration

Goethite potentiometric titrations were carried out at 0.1 M $NaNO_3$ and 10 g/L following the method of Hayes et al. (1991). Detailed experimental procedure is reported in Peacock and Sherman (2004a,b). We report an experimental pH_{PZC} (the pH where the surface charge is zero) of 9.18. This lies within the range of reported experimental values (~8–9.5).

2.3. pH adsorption edge experiments

Goethite batch experiments were prepared with U(VI) aqueous solution using AR grade reagents and all adsorption experiments were conducted at 25 °C. pH measurements were calibrated to ±0.05 pH units using Whatman NBS grade buffers. U(VI) stock solution was prepared at 100 ppm from $UO_2(NO_3)_2 \cdot 6H_2O$ in 0.01 M HNO_3. Goethite stock suspensions were prepared from air-dried goethite at 10 g/L. $NaNO_3$ stock solution was prepared at 0.1 M for use as background electrolyte.

Three sorption edges were measured under conditions where $p(CO_2) < 10^{-6.0}$ bar (1 ppm CO_2). For these experiments, stock solutions and a goethite suspension were prepared with pre-boiled, N_2(g) (<1 ppm CO_2(g)) purged 18.2 MΩ MilliQ water and purged with N_2(g) (<1 ppm CO_2(g)) prior to use. Adsorption edge experiments at 1×10^{-7} mol/L (0.024 ppm), 1×10^{-6} mol/L (0.24 ppm) and 1×10^{-5} mol/L (2.4 ppm) $[U]_{total}$ were prepared by

adding 44.58, 44.48 and 43.49 mL of background electrolyte and 11, 110 and 1100 μL of U(VI) stock solution, respectively, to polypropylene centrifuge tubes containing 410 μL aliquots of the goethite slurry. Total volume was therefore 45 mL and solid/solution ratio was 0.09 g/L. Initial pH of the resulting suspensions was recorded and suspension pH was then varied from pH ~3–9.5 by the dropwise addition (<0.5 mL total) of HNO_3/NaOH and recorded after stabilisation to two decimal places. Initial pH was always below that required for precipitation of schoepite. Addition of experimental solutions and pH adjustments of resulting suspensions were performed under N_2(g) (<1 ppm CO_2(g)) and with constant stirring. To avoid possible precipitation of schoepite at 1×10^{-6} mol/L and 1×10^{-5} mol/L $[U]_{total}$, U(VI) stock solution was added incrementally. Adsorption edge experiments were then purged and sealed under N_2(g) (<1 ppm CO_2(g)) and rotated continuously for 48 h.

Three sorption edges were determined under conditions where $p(CO_2) = 10^{-3.5}$ bar. Adsorption edge experiments at 1×10^{-6} mol/L and 1×10^{-5} mol/L $[U]_{total}$ were prepared by adding 44.48 and 43.49 mL of background electrolyte, respectively, to polypropylene centrifuge tubes containing 410 μL aliquots of a goethite slurry. pH measurements and adjustments were made following the method above but were not performed under N_2(g) (<1 ppm CO_2(g)). Dropwise addition of HNO_3/NaOH was <0.5 mL total. For experiments at pH > 7, sufficient $NaHCO_3$ was added to achieve equilibrium with air at the desired experimental pH. The pH of the suspension was adjusted to the desired experimental value immediately before and after $NaHCO_3$ addition. Centrifuge tubes were then rotated for 24 h and opened regularly to keep the system open to the atmosphere. pH was then remeasured but not adjusted: drift was less than 0.15 pH units. Experiments at 1×10^{-6} mol/L and 1×10^{-5} mol/L $[U]_{total}$ were completed by adding 110 and 1100 μL of U(VI) stock solution, respectively. Total volume was therefore 45 mL and solid/solution ratio was 0.09 g/L. pH was again remeasured but not adjusted: drift was less than 0.15 pH units. To avoid possible precipitation of schoepite at 1×10^{-5} mol/L $[U]_{total}$, U(VI) stock solution was added incrementally. Adsorption edge experiments were then rotated for 48 h and opened regularly to keep the system open to the atmosphere.

Final pH measurements were measured for the experimental suspensions before centrifugation or filtering. Adsorption edge experiments were then centrifuged (10,000 rpm for 5 min) to produce a clear supernate for determination of total uranium concentration. Samples for EXAFS were centrifuged (10,000 rpm for 15 min) to produce an adsorption sample (thick paste) and a clear supernate for determination of total uranium concentration. Supernates were filtered using 0.2 μm cellulose nitrate membrane filters, acidified with 1% HNO_3 and analysed for uranium by inductively-coupled plasma mass spectrometry (ICP-MS). Thick paste adsorption samples for EXAFS were storage at 1–4 °C for a maximum of 48 h before scanning.

2.4. EXAFS spectra of U sorption complexes

EXAFS data were collected at the CCLRC Synchrotron Radiation Source at Daresbury Laboratory, U.K. Spectra of the U L_{III}-edge (17.167 keV) were collected on station 16.5 which is designed for measurements on ultra-dilute systems. During data collection, storage ring energy was 2.0 GeV and the beam current varied between 130 and 240 mA. Adsorption samples were presented to the X-ray beam as a wet paste held in a 2 mm-thick Teflon slide with a 4×10 mm sample slot. Small sheets of 250 μm-thick Mylar were placed on either side of the Teflon slide and sealed with a small amount of vacuum grease to hold the wet pastes in place and prevent drying of the samples. EXAFS data were collected from up to 20 fluorescence mode scans using an Ortec 30-element solid-state detector.

EXAFS data reduction was performed using Daresbury Laboratory software (EXCALIB, and EXBACK, Dent and Mosselmans, 1992). EXCALIB was used to calibrate from monochromator position (millidegrees) to energy (eV) and to average multiple spectra from individual samples. EXBACK was used to define the start of the EXAFS oscillations (determined from the inflection point on the L_{III} edge) and perform background subtraction. The pre-edge was fit to a linear function and the post-edge background to two 2nd-order polynomial segments. The phase-shifts and potentials were calculated in the small atom (plane-wave) approximation and we allowed for multiple scattering as coded in EXCURV98 (Binsted, 1998). The phase-shift functions used in the curve fitting were derived by *ab initio* methods in EXCURV98 using Hedin–Lundqvist potentials (Hedin and Lundqvist, 1969) and von Barth ground states. No Fourier filtering was performed during the data analysis.

2.5. Density functional calculations

Quantum mechanical calculation of cluster geometries and energies were done using the ADF code of te Velde et al. (2001). ADF implements density functional theory for finite clusters and molecules using the linear combination of atomic orbital formalism. For all atoms except hydrogen, we used frozen core orbitals (i.e., 1s, 2s, 2p and 3p for Fe; 1s for O and 1s to 5p for U). Scalar relativistic corrections were applied using the zeroth-order regular approximation (ZORA) of Faas et al. (1995). Molecular orbitals in the ADF code are constructed from Slater type atomic orbitals which consist of a cartesian part $r^{kr}x^{kx}y^{ky}z^{kz}$ with $k_x + k_y + k_z = l$(l = angular momentum quantum number) and an exponential part e^{-ar}. For all atoms, we used an uncontracted, triple-zeta basis set with polarization functions; the basis set is modified to describe the core-like functions in the ZORA formalism. No optimization of the basis set was done. Counterpoise corrections for basis set superposition energy were found to be negligible (<1 kJ/mol).

The calculations were done in the generalized gradient approximation (GGA) of the exchange-correlation functional (Perdew et al., 1992) using the PBE functional (Perdew et al., 1996). All calculations were done using the

Table 1
U(VI) solution reactions

Solution species	Reaction	Log equilibrium constant* ($I = 0.1$)**
UO_2^{2+}	UO_2^{2+}	—
UO_2OH^+	$UO_2^{2+} + H_2O = UO_2OH^+ + H^+$	−5.20 (−5.45)
$UO_2(OH)_2^0$	$UO_2^{2+} + 2H_2O = UO_2(OH)_2^0 + 2H^+$	−12.15 (−12.43)
$UO_2(OH)_3^-$	$UO_2^{2+} + 3H_2O = UO_2(OH)_3^- + 3H^+$	−20.25 (−20.34)
$UO_2(OH)_4^{2-}$	$UO_2^{2+} + 4H_2O = UO_2(OH)_4^{2-} + 4H^+$	−32.40 (−32.07)
$(UO_2)_2(OH)^{3+}$	$2UO_2^{2+} + H_2O = (UO_2)_2(OH)^{3+} + H^+$	−2.70 (−2.54)
$(UO_2)_2(OH)_2^{2+}$	$2UO_2^{2+} + 2H_2O = (UO_2)_2(OH)_2^{2+} + 2H^+$	−5.62 (−5.90)
$(UO_2)_3(OH)_4^{2+}$	$3UO_2^{2+} + 4H_2O = (UO_2)_3(OH)_4^{2+} + 4H^+$	−11.90 (−12.46)
$(UO_2)_3(OH)_5^+$	$3UO_2^{2+} + 5H_2O = (UO_2)_3(OH)_5^+ + 5H^+$	−15.55 (−16.36)
$(UO_2)_3(OH)_7^-$	$3UO_2^{2+} + 7H_2O = (UO_2)_3(OH)_7^- + 7H^+$	−32.2 (−32.85)
$(UO_2)_4(OH)_7^+$	$4UO_2^{2+} + 7H - 2O = (UO_2)_4(OH)_7^+ + 7H^+$	−21.90 (−22.99)
$UO_2CO_3^0$	$UO_2^{2+} + H_2CO_3 = UO_2CO_3^0 + 2H^+$	−6.74 (−7.02)
$UO_2(CO_3)_2^{2-}$	$UO_2^{2+} + 2H_2CO_3 = (CO_3)_2^{2-} + 4H^+$	−16.75 (−16.42)
$UO_2(CO)_3^{4-}$	$UO_2^{2+} + 3H_2CO_3 = UO_2(CO)_3^{4-} + 6H^+$	−28.2 (−26.34)
$(UO_2)_2CO_3(OH)_3^-$	$2UO_2^{2+} + H_2CO_3 + 3H_2O = (UO_2)_2CO_3(OH)_3^- + 5H^+$	−17.55 (−17.92)
$(UO_2)_3CO_3(OH)_3^+$	$3UO_2^{2+} + H_2CO_3 + 3H_2O = (UO_2)_3CO_3(OH)_3^+ + 5H^+$	−16.04 (−16.85)
$(UO_2)_{11}(CO_3)_6(OH)_{12}^{2-}$	$11UO_2^{2+} + 6H_2CO_3 + 12H_2O = (UO_2)_{11}(CO_3)_6(OH)_{12}^{2-} + 24H^+$	−63.74 (−66.20)
$(UO_2)_3(CO_3)_6^{6-}$	$3UO_2^{2+} + 6H_2CO_3 = (UO_2)_3(CO_3)_6^{6-} + 12H^+$	−46.08 (−42.34)

* Grenthe et al. (1992) and Guillaumont et al. (2003).
** Calculated using the Davies equation.

spin-unrestricted formalism to account for the five unpaired 3d-electrons of iron and the two Fe atoms were set up in a ferromagnetic configuration.

To account for the long-range solvation field we used the Conductor-like Screening model (COSMO) (Klamt and Schuurmann, 1993; Klamt, 1995; Klamt and Jonas, 1996). Here, the complex is surrounded by a solvent-accessible surface and embedded in a dielectric continuum which is a perfect conductor ($\varepsilon = \infty$). The solvent accessible surface is defined by surrounding each atom by a sphere of radius $R_a = 1.17 * R_a^{vDW}$ (where R_a^{vDW} is the van der Waals radius of the atom) as optimized by Klamt et al. (1998). This gives radii of 1.72 Å for O and 2.05 Å for Cl. The radius of the solvent is 1.3 Å for H_2O. Polarization of the dielectric continuum yields a charge density (the "screening charge density") surrounding the molecule. The screening charge density mimics the effect of the solvent. The solvation energy is determined by scaling the COSMO energy by $f(\varepsilon) = (\varepsilon - 1)/(\varepsilon + 1/2)$ where ε is the dielectric constant of the solvent (78.8 for water at 25 °C).

The geometries of the clusters were optimized using a Newton–Raphson method and Broydon–Fletcher update of the Hessian matrix as coded in ADF. The total energies of each complex during geometry optimizations were converged to ±0.3 kJ/mol.

2.6. Surface complexation modelling

Surface complexation modelling was done using a FORTRAN program (EQLFOR)[1] based on the original "tableau" speciation algorithm described by Morel and Morgan (1972). Modifications to the mass balance, Jacobian and convergence routines were made to include the surface and diffuse layer charges of the basic (2 layer) or extended (3 layer) Stern model. Equilibrium constants for surface complexes were derived by fitting sorption edges to 1–2 surface complexation equilibria but also including the equilibria given in Table 1. The speciation routines are called by a gradient search fitting algorithm (Bevington and Robinson, 2002) to optimize the equilibrium constants. The fitting was obtained by minimizing χ^2 which is calculated assuming a relative error of 2% in concentrations/pH.

In the Morel and Morgan (1972) method, the speciation is calculated using mass balance constraints to give the molal concentrations of surface species. The correct thermodynamic formulation (i.e., one that gives the correct ideal configurational entropy of a species) of the activity of a surface species is in terms of the mole fraction of surface sites occupied by the species. The resulting stability constants are obtained from the apparent (fitting to mass balance) stability constants by converting the concentration of each surface species to its mole fraction. Ionic strength corrections to the stability constants for aqueous species were made using the Davies equation.

3. RESULTS AND DISCUSSION

3.1. Sorption of U on goethite

Sorption edges of U on goethite as a function of surface loading and $P(CO_2)$ are shown in Fig. 2. Also shown are the model fits based on the surface complexes discussed below. The solution speciation (Figs. 3 and 4) suggests the formation of $UO_2(OH)_n$ complexes above pH 6. For $[U]_{tot} > 10^{-7}$, schoepite will precipitate near pH 7.

The presence of CO_2 has a dramatic effect on the sorption of U(VI). As observed in previous studies (e.g., Hsi and Langmuir, 1985; Waite et al., 1994; Duff and Amrhein, 1996),

[1] Input files and the source code are available as an electronic annex.

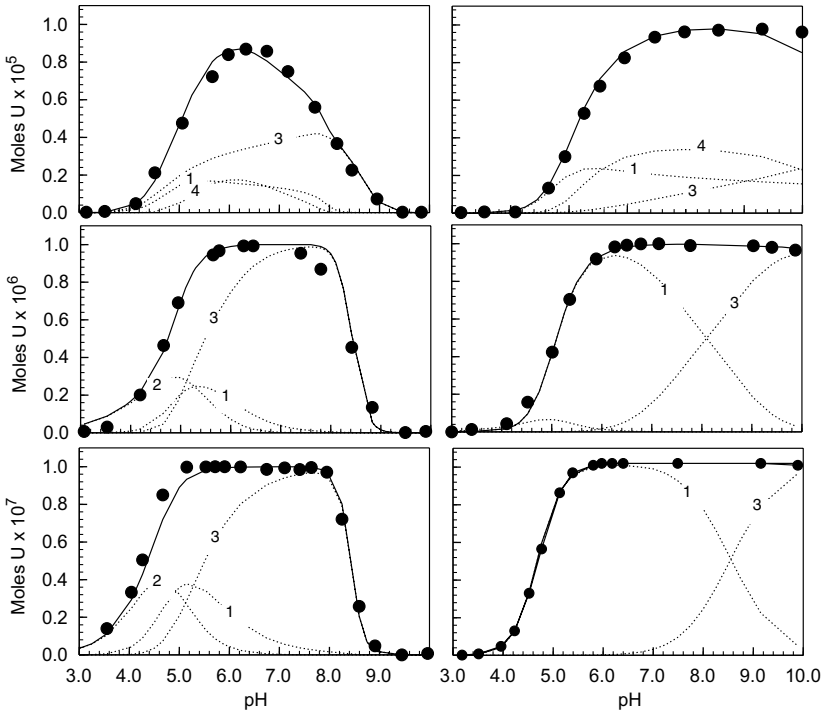

Fig. 2. Sorption of U(VI) to FeOOH as a function of maximum surface loadings (top: 2.6 wt% top; middle: 0.26 wt%, bottom: 0.026 wt%) and P(CO_2) (left: $10^{-3.5}$ bar, right: $<10^{-6}$ bar). Complex 1 is $(>FeOH)_2UO_2$. Complex 2 is $(>FeOH)_2UO_2CO_3$. Complex 3 is the proposed $>FeOCO_2UO_2$. Complex 4 is a dimer $(>FeOH)_2(UO_2)_2(OH)_2$. Symbols are experimental data and lines are model fits.

sorption edges obtained in the presence of ambient CO_2 show a strong desorption of UO_2 at pH > 7; this results from the formation of strong UO_2CO_3 complexes in solution (Fig. 4). What has not been observed in previous studies is the enhanced sorption of UO_2^{2+} at low pH < 6 in the presence of CO_2. This may be either an electrostatic effect resulting from surface sorbed CO_3^{2-} or may result from the formation of a ternary complex such as $>FeOCO_2UO_2$ or $(>FeOH)_2UO_2CO_3$. Such complexes are unexpected insofar as UO_2^{2+} does not form any UO_2CO_3 complexes below pH 6.

3.2. EXAFS of U(VI) sorbed to goethite

EXAFS spectra of UO_2^{2+} sorbed to goethite are shown in Fig. 5. The three-dimensional coordination environment about the U atom was modelled using a cluster with C2 symmetry (Fig. 6). This allows for the full multiple scattering analysis with the smallest number of independent parameters. Lowering the symmetry to C_1 and treating each atom independently did not statistically improve the EXAFS fits. Thompson et al. (1997) found multiple scattering in U L_{III} edge spectra to be unimportant beyond $k = 3$ Å^{-1}. However, we find multiple scattering interferes with fits to the U–Fe single scattering peaks. The calculated fit parameters are given in Table 2. As expected, adsorbed U(VI) has 2 axial oxygens at 1.8 Å and 4–5 equatorial oxygens at ~2.3–2.5 Å. The Fourier transforms of the spectra show a shoulder on the hydration peak that suggests a ligand near 2.8–2.9 Å. Bargar et al. (1999, 2000) have interpreted an analogous feature in the spectrum of UO_2^{2+} on hematite as resulting from a U–C scattering in a ternary UO_2CO_3 complex. Ulrich et al. (2006) find that the 2.9 feature is also present in the EXAFS of UO_2^{2+} sorbed to ferrihydrite at pH 8 when $pCO_2 = 10^{-3.5}$ bar. Furthermore, they find evidence for the expected carbonate oxygen at 4.3 Å. On the other hand, Ulrich et al. (2006) also find the 2.8–2.9 Å peak (but without the 4.3 Å oxygen) at pH 5.5 when $pCO_2 < 2 \times 10^{-6}$ bar. Ulrich et al. (2006) proposed that the 2.9 Å ligand is an oxygen on the surface FeO_6 polyhedron; however, the structure they proposed requires a physically unrealistic distance between the UO_2^{2+} axial oxygen and the FeO_6 surface oxygens. Even if the E2 complex occurs on ferrihydrite, it cannot explain the 2.9 Å peak in goethite where the E2 complex cannot be significant at high surface loading. We find the same 2.9 Å peak on goethite at pH 5.5 in $pCO_2 = 10^{-3.5}$ with no evidence for a carbonate oxygen at 4.3 Å. For our sample at pH 5.5, we find that we can also model the shoulder as a splitting of the UO_2^{2+} hydration shell with an O at 2.55 Å (Fig. 5 and Table 2). On the other hand, our surface complexation model predicts UO_2–CO_3 ternary complexes at pH 5.5 at low surface loading. Consequently, we suspect that the 2.9 Å feature in the EXAFS at pH 5.5 may also result from U–C scattering.

In all spectra, the Fourier transform shows a peak near 3.48 Å that has been attributed by previous workers to a bidentate edge-sharing (E2) inner-sphere complex (e.g., Waite et al., 1994; Bargar et al., 1999; Moyes et al., 2000; Ulrich et al., 2006). However, for all of our samples (surface loading 0.21–2.6 wt% U), we can fit the ~3.48 Å peak entirely to multiple scattering within the cluster shown in Fig. 6 (primarily paths 1, 2 and 6 in Table 3). The Fourier transform of the spectrum of metaschoepite (Fig. 4) also

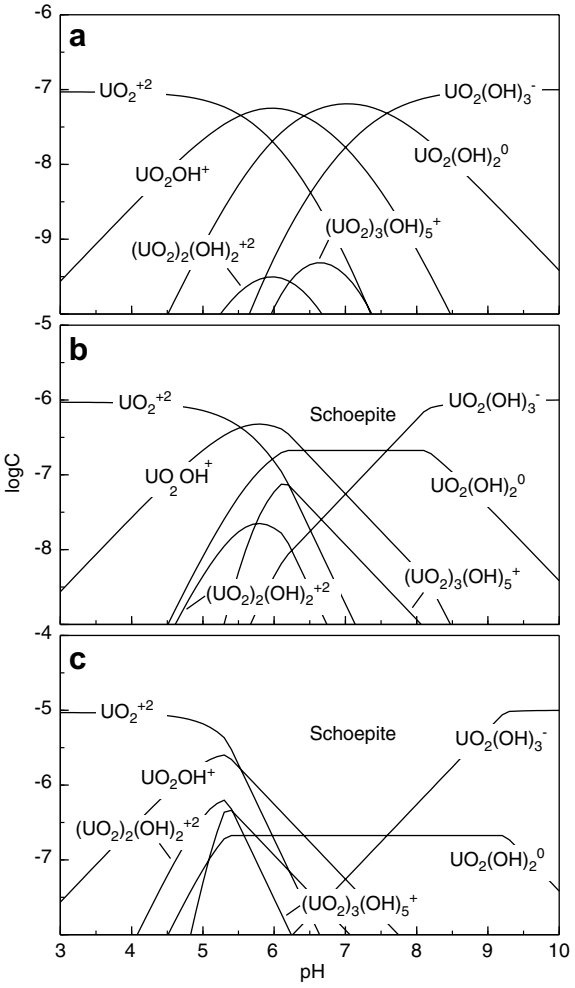

Fig. 3. Aqueous speciation of U(VI) in the absence of CO_2 as a function of pH. $I = 0.1$ M. (a) 1×10^{-7} mol/L $[U]_{total}$ (b) 1×10^{-6} mol/L $[U]_{total}$ (c) 1×10^{-5} mol/L $[U]_{total}$. (Data from Grenthe et al., 1992 and Guillaumont et al., 2003.)

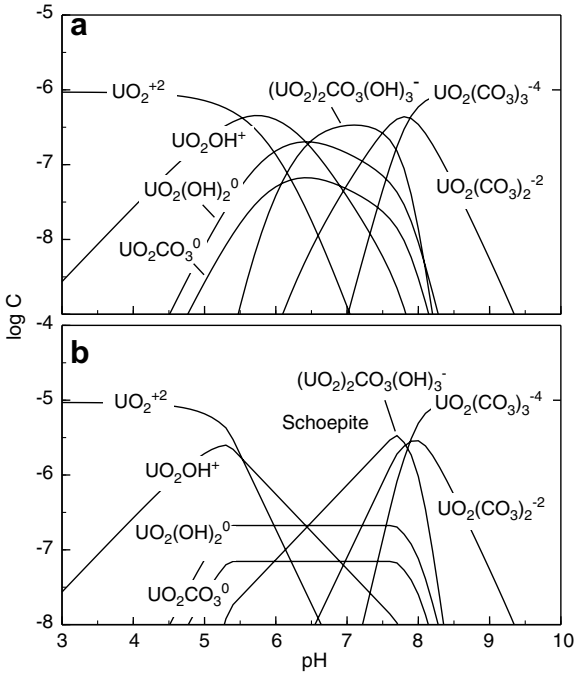

Fig. 4. Aqueous speciation of U(VI) in an open system equilibrated with $p(CO_2) = 10^{-3.5}$ as a function of pH. $I = 0.1$ M. (a) 1×10^{-6} mol/L $[U]_{total}$ (b) 1×10^{-5} mol/L $[U]_{total}$. (Data from Grenthe et al., 1992 and Guillaumont et al., 2003.)

shows a clear peak at 3.48 Å even though there is no U–O or U–U distance near that value in the metaschoepite structure. (We did not fit the metaschoepite with full multiple scattering as there are several different U sites in the structure.) Even when the surface loading is only 0.21 wt% U, we cannot find any statistical evidence (decreased χ^2) for the E2 complex. This supports our hypothesis that the E2 complex is only a small, if any, fraction of surface-sorbed U. Accordingly, there should be evidence for an alternative, dominant, complex such as the bidentate corner-sharing (C2) complex described above. Based on our DFT calculations (discussed below), we expect the C2 complex to give a U–Fe scattering near 4.2 Å. In the Fourier transforms of the EXAFS spectra, however, any peak near 4.2 Å suggestive of a C2 complex is weak and difficult to resolve from the noise. To resolve U–Fe scattering at this distance requires reasonable signal to noise out to $k = 14$ Å^{-1}. More significantly, however, is that a that multiple scattering involving the Fe atoms (paths 30 and 31, Table 3) interferes with the U–Fe scattering in the C2 complex. This effect is demonstrated in Fig. 7 and results from the shadowing of atoms when the path angles are ~180 ° (Table 3). Unfortunately, because of weak single scattering and interference from multiple scattering, EXAFS spectra are of limited utility in resolving the next-nearest neighbour coordination environment of U. Inclusion of the Fe next-nearest neighbor shell (as in Table 2) usually gives little improvement (1–2%) in the goodness of fit parameter R. By characterising the first coordination shell, however, we are able to provide useful constraints for the surface complexation model discussed below.

Evidence for U–U distances associated with polynuclear complexes in the EXAFS at high surface loading is weak. At pH 8, a 1×10^{-5} mol/L solution of U would be oversaturated with respect to schoepite $(UO_2)_8O_2(OH)_{12}(H_2O)_{12}$ if sorption on goethite did not occur. The schoepite structure has next-nearest-neighbour U–U distances from 3.829 to 4.510 Å (Finch et al., 1996). The EXAFS spectrum of schoepite (Fig. 8) shows U–U scattering corresponding to these distances. Analogous U–U scattering peaks are absent from the spectra of UO_2^{2+} on goethite suggesting no surface precipitate or polynuclear complexes have formed. Furthermore, the short U–U distance in schoepite results from oxy-bridged UO_2^{2+} ions which also give a short U–O distance of 2.17 Å in the second coordination shell. Such a short U–O distance is not resolved in our data. The absence of schoepite precipitation implies that sorption of UO_2^{2+} onto FeOOH is favoured.

3.3. First-principles models of surface complexation

Several quantum mechanical studies at different levels of theory predict that the UO_2^{2+} aquo complex exists as

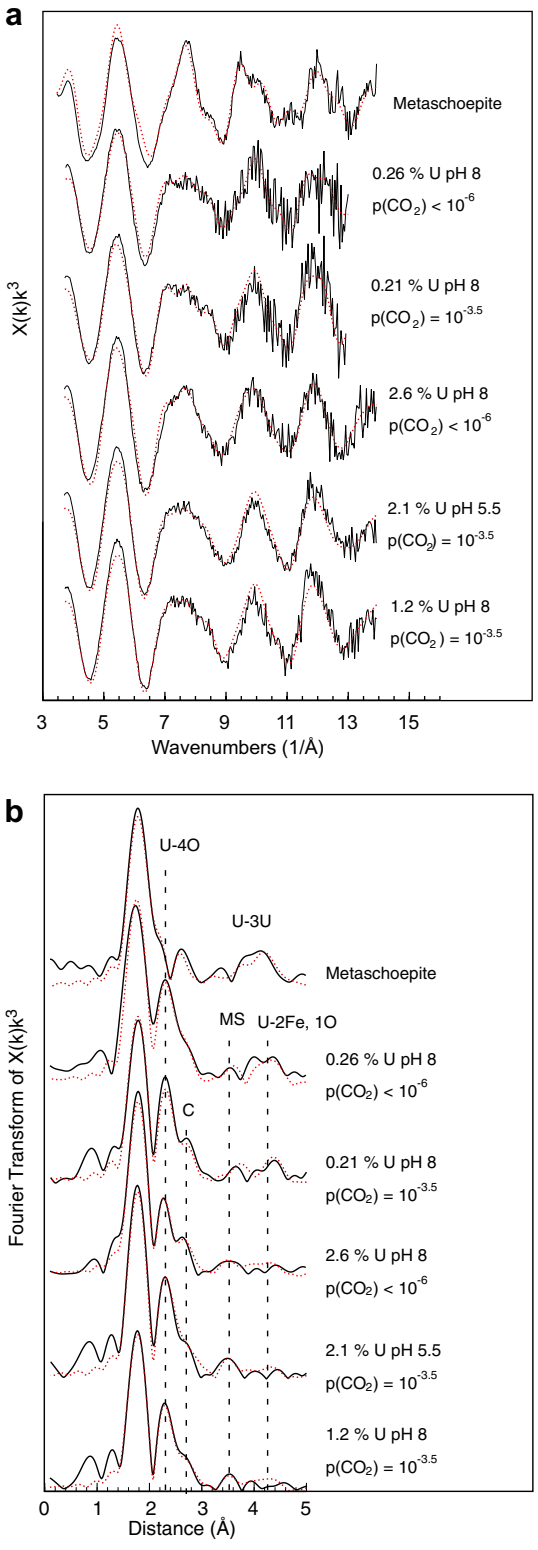

Fig. 5. (a) EXAFS spectra and (b) Fourier transforms of U(VI) sorbed onto goethite. The Fourier transforms calculated using EXCURV98 (Binsted, 1998) are corrected by U–O scattering phase shifts to give approximate actual distances.

$UO_2(H_2O)_5^{2+}$ (Farkas et al., 2000; Hay et al., 2000; Moskaleva et al., 2004). These results showed good agreement

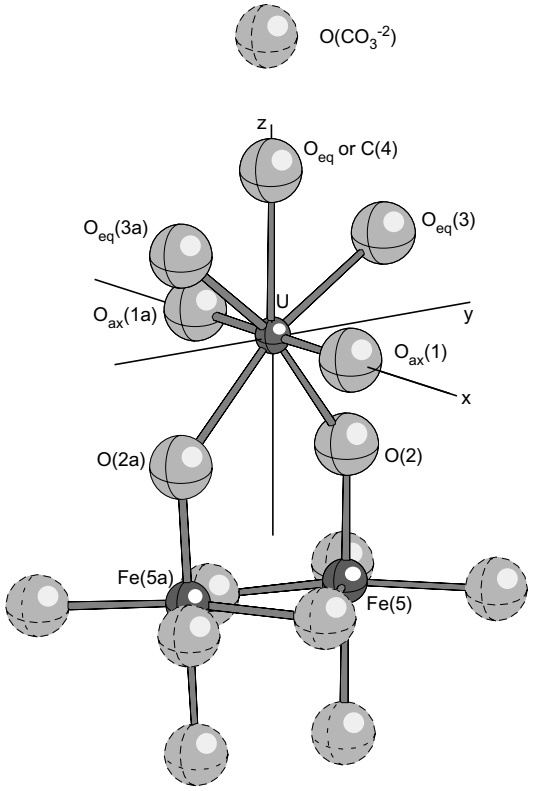

Fig. 6. Cluster used in EXAFS fits for U(VI) sorbed to goethite.

with EXAFS studies on UO_2^{2+} aqueous complexes (e.g., Allen et al., 1997). Molecular-dynamical simulations of UO_2^{2+} hydration based on classical potentials (Druchok et al., 2005) indicate 5 H_2O, OH^- ligands coordinating to the UO_2^{2+} ion. Our calculated geometries for $UO_2(H_2O)_6^{2+}$ and $UO_2(OH)(H_2O)_5^{+}$ complexes are shown in Fig. 8a and b. We also find that UO_2^{2+} adopts a fivefold coordination with a U–OH_2 bond lengths ranging from 2.38 to 2.53 Å. In the $UO_2(OH)(H_2O)_5^{+}$ complex, there is a large splitting in U–O bond lengths of 2.14 (U–OH) and 2.5 (U–OH_2). In accordance with these results we assumed that surface-complexed UO_2^{2+} is surrounded by 5 ligands.

We can model both the E2 and C2 complexes using $Fe_2(OH)_4(H_2O)_6UO_2(OH,\ H_2O)_3$clusters (Fig. 8c and d). The calculated bond-lengths and geometries are in reasonable agreement with those observed from the EXAFS spectra (discussed below). Note that the calculations predict that a U–OH distance will 2.1–2.2 Å; the EXAFS give no evidence for such a short first-shell distance and suggest that no terminal OH are coordinated to U. The persistence of the hydration shell in the geometry optimizations indicates that surface complexed UO_2^{2+} also has fivefold coordination for the C2 $(>FeOH)_2UO_2(H_2O)_3$ and E2 $>Fe(OH)_2UO_2(H_2O)_3$ surface complexes. In passing, we note that Steele et al. (2002) have used classical shell-model potentials to predict the structure of UO_2^{2+} surface complexes. Their predicted structure of the bidentate corner-sharing complex (analogous to that in Fig. 8c), however, has an unrealistically low Fe–U distance of 3.4–3.49 Å.

Table 2
U coordination environment from fits to U L_{III}-edge EXAFS spectra at 298 K

		2 O (UO_2)	2 **O**(Fe–OH)	2 **O**(H_2O or CO_3^{2-})	1 **C**(CO_3^{2-}) or 1 **O** (H_2O)	1 **O**(CO_3)	2 **Fe**	*R*
pH 8.0	*R*	1.80	2.33	2.46	**C** at 2.93	4.28	4.31	38
0.21 wt% U	ϕ, θ	*90, 0*	*127, 0*	*54, 90*	*0, 0*	*0, 0*	*140, 90*	
$p(CO_2) < 10^{-6.0}$	$2\sigma^2$	0.004	0.003	0.001	0.002	0.005	0.008	
pH 8.0	*R*	1.80	2.34	2.48	**C** at 2.92	4.25	4.31	33
0.21 wt% U	ϕ, θ	*90, 0*	*127, 0*	*54, 90*	*0, 0*	*0, 0*	*140, 90*	
$p(CO_2) = 10^{-3.5}$	$2\sigma^2$	0.003	0.001	0.003	0.003	0.01	0.01	
pH 8.0	*R*	1.81	2.33	2.46	**C** at 2.91	4.4	4.35	27
2.6 wt% U	ϕ, θ	*90, 0*	*127, 0*	*54, 90*	*0, 0*	*0, 0*	*140, 90*	
$p(CO_2) < 10^{-6}$	$2\sigma^2$	0.005	0.009	0.01	0.006	0.01	0.015	
pH 5.5	*R*	1.80	2.32	2.41	**O** at 2.54	—	4.35	25
2.1 wt% U	ϕ, θ	*90, 0*	*127, 0*	*54, 90*	*0, 0*	—	*140, 90*	
$p(CO_2) = 10^{-3.5}$	$2\sigma^2$	0.004	0.009	*0.005*	*0.005*	—	0.015	
pH 8.0	*R*	1.81	2.35	2.47	**C** at 2.91	4.28	4.27	33
1.2 wt% U	ϕ, θ	*90, 0*	*127, 0*	*54, 90*	*0, 0*	*0, 0*	*140, 90*	
$p(CO_2) = 10^{-3.5}$	$2\sigma^2$	0.003	0.001	*0.003*	0.003	0.011	0.009	

*Values in italics are constrained. ϕ and θ are the spherical coordinates defined as the angles from the *z* and *x* axes in Fig. 6. For all spectra, including the Fe shell improves changes *R* by <2%.

Table 3
Multiple scattering pathways

Path	Multiplicity	Path*	Distance (Å)	Angle	Amplitude
1	2	0-1-0-1-0	7.228	0	0.042038
2	2	0-1-0-1a-0	7.228	180	0.054776
3	8	0-1-0-2-0	8.264	90	0.02402
4	8	0-1-0-3-0	8.511	90	0.021318
5	4	0-1-0-4-0	9.474	90	0.005102
6	2	0-1-1a-0	7.228	180	0.040976
7	8	0-1-2-0	7.077	90	0.041998
8	4	0-1-2-1-0	9.503	52.1	0.004848
9	4	0-1-2-1a-0	9.503	180	0.001838
10	8	0-1-2-4-0	9.669	90	0.001213
11	8	0-1-3-0	7.299	90	0.038133
12	4	0-1-3-1-0	9.7	53.6	0.005174
13	4	0-1-3-1a-0	9.7	180	0.002047
14	4	0-1-4-0	8.18	90	0.01023
15	8	0-1-4-2-0	9.562	90	0.00167
16	2	0-2-0-2-0	9.3	0	0.005609
17	2	0-2-0-2a-0	9.3	85	0.002434
18	4	0-2-0-3-0	9.547	79	0.003797
19	4	0-2-0-3a-0	9.547	164.1	0.015946
20	2	0-2-2a-0	7.792	85	0.005761
21	4	0-2-3-0	7.813	79	0.009056
22	4	0-2-3a-0	9.501	164.1	0.017186
23	4	0-2-4-0	7.242	85.2	0.006271
24	2	0-2-4-2-0	8.624	85.2	0.00089
25	2	0-4-2-4-0	9.835	52.3	0.001939
26	2	0-2-4-2a-0	8.624	104.5	0.000457
27	2	0-3-0-3-0	9.794	0	0.00676
28	2	0-3-0-3a-0	9.794	116.9	0.000333
29	2	0-3-3a-0	9.07	116.9	0.00203
30	4	0-3-5-0	8.62	140.4	0.04883
31	2	0-3-5-3-0	8.879	140.4	0.009538

* Atom numbers given as in Fig. 6.

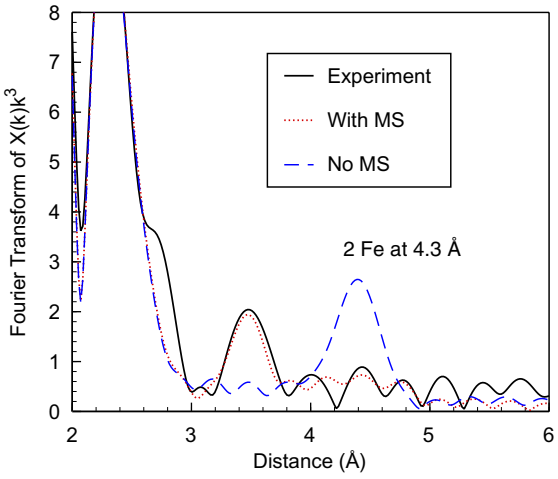

Fig. 7. Effect of multiple scattering on features in the Fourier transform of EXAFS (2.1 wt% U on goethite, pH 5.5 and $pCO_2 = 10^{-3.5}$). Multiple scattering completely accounts for the feature at 3.5 Å that would have been assigned to the E2 complex. Inclusion of the C2 complex yields a peak near 4.4 Å that is strongly masked when multiple scattering is included.

As shown in Fig. 8c, the U–Fe distance in the bidentate corner-sharing (C2) complex is much larger. Only the edge-sharing (E2) complex has a U–Fe distance near 3.5 Å. Why the classical shell-model potentials gave such a short U–Fe distance for the C2 complex is unclear.

Since clusters modelling the E2 and C2 complexes have the same stoichiometry, we can compare their energies. In the absence of the COSMO solvation field, the corner-sharing (C2) $Fe_2(OH)_4(H_2O)_6UO_2OH(H_2O)_2$ cluster is calculated to be 0.24 eV (23 kJ/mol) less stable than the edge-sharing (E2) $Fe_2(OH)_4(H_2O)_6UO_2OH(H_2O)_2$ cluster. With the COSMO solvation field, the energy difference decreases to 0.12 eV (12 kJ/mol). Since the difference in zero-point energy and vibrational enthalpy between clusters can be neglected, the static internal energy difference can be equa-

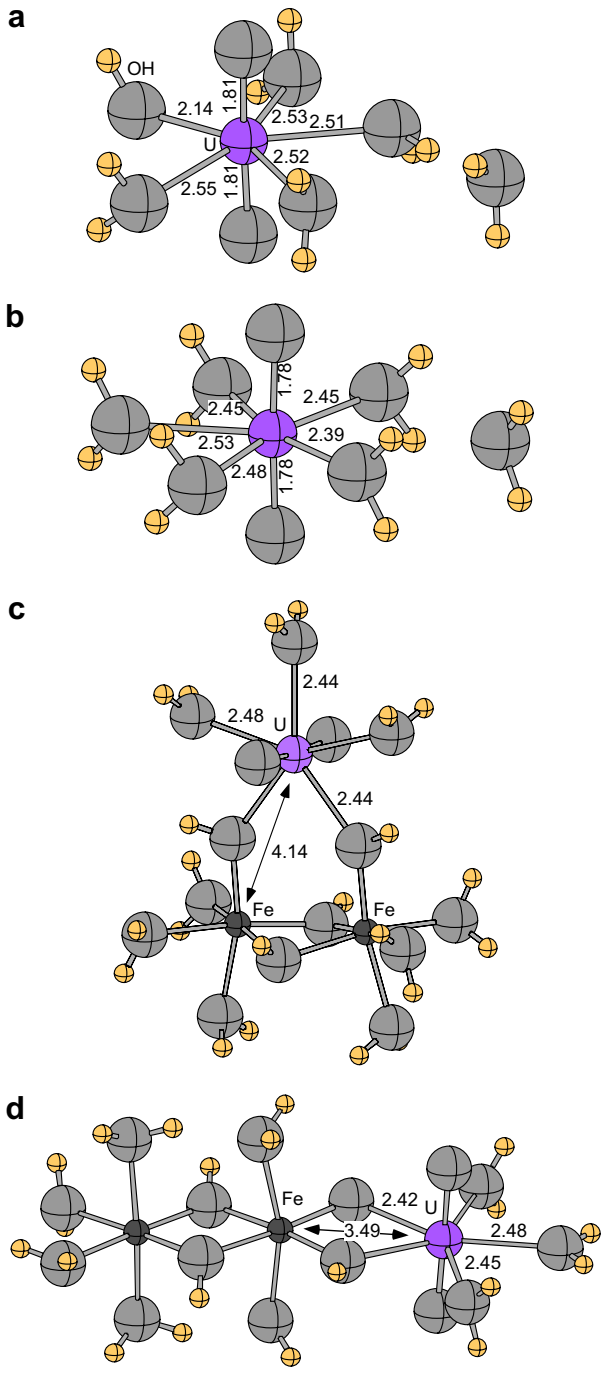

Fig. 8. U(VI) ab initio molecular geometry clusters. (a) $UO_2(H_2O)_6^{2+}$ complex, (b) $UO_2(OH)(H_2O)_5^{+}$ complex, (c) bidentate corner-sharing mononuclear cluster on (predominantly) {101} and (d) bidentate edge-sharing mononuclear cluster on {210} or {010}. Bond lengths shown in Å.

ted to an enthalpy difference of ~12 kJ/mol at 1 bar. This, in turn implies that the log K for the E2 and C2 complexes should differ by ~2 log units at 298 K. However, this neglects the difference between the electrostatic potentials of the {210} and {101} surfaces in the real system. If the two complexes are indeed so similar in energy, then configurational entropy will favour a significant proportion of C2 complexes even at low surface coverage because the number of C2 sites is much greater.

Both EXAFS spectra and the observed effect of CO_2 on U sorption are consistent with $>FeOCO_2UO_2(H_2O)_3$ or $(>FeOH)_2UO_2CO_3$ ternary complexes. Optimized geometries of clusters used to model these complexes are shown in Fig. 9. These predict that the equatorial plane will have 4 ligands and be split into two U–O distances near 2.3–2.4 and 2.5 Å. This is in good agreement with the EXAFS of UO_2^{2+} sorbed in the presence of CO_2. Both clusters, however, give a U–C distance that is ~0.1 Å too short. A similar error is found for calculated geometries of the $UO_2(CO_3)_3^{4-}$ complex (Majumdar et al., 2003).

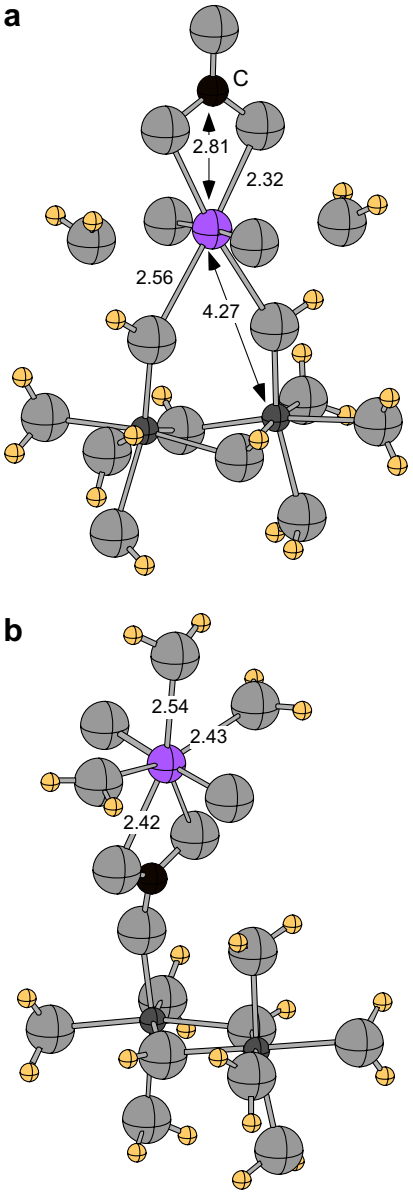

Fig. 9. Predicted structures of possible ternary complexes (a) $(>FeOH)_2UO_2CO_3$ and (b) $>FeOCO_2UO_2(H_2O)_3$.

3.4. Surface complexation modelling

3.4.1. Surface site densities and surface protonation

As discussed by previous workers (e.g., Randall et al., 1999; Boily et al., 2001), goethite crystallites are acicular needles dominated by the {101} and terminated by {210} and {010}. On the {210} surfaces there are 10.8 Fe–OH sites/nm^2. On the {101} surfaces, there are 3.03 Fe–OH sites/nm^2 and 2.78 Fe_3O sites/nm^2. Following Hiemstra and Van Riemsdijk (1996) we will assume that the Fe_3O sites will only sorb protons. If we assume that the {210} and {010} termination surfaces comprise only ~1% of the total surface area, then there are ~28 {101} >FeOH sites for every {210} site. Assuming the proton affinities of {210} $>Fe(OH)_2$ sites are similar to those of {101} >FeOH sites, it will not be possible to resolve the protonation of the {210} and {110} surfaces. On the {101} surfaces the protonation equilibria will be

$$> \mathrm{FeOH}^{-1/2} + \mathrm{H}^+ = > \mathrm{FeOH_2}^{+1/2} \quad (1a)$$

$$K_{a1} = \frac{X_{\mathrm{FeOH_2^{+0.5}}}}{X_{\mathrm{FeOH^{-0.5}}}[\mathrm{H}^+]\gamma_{H^+}} \exp(-\psi_0 F/RT)$$

$$> \mathrm{Fe_3O}^{-1/2} + \mathrm{H}^+ = > \mathrm{Fe_3OH}^{+1/2} \quad (1b)$$

$$K_{a2} = \frac{X_{\mathrm{Fe_3OH^{+0.5}}}}{X_{\mathrm{Fe_3O^{-0.5}}}[\mathrm{H}^+]\gamma_{\mathrm{H}^+}} \exp(-\psi_0 F/RT)$$

where ψ_0 is the surface electrostatic potential, R is the gas constant, F is the Faraday constant and T is temperature. Here, and in what follows, we define the (ideal) activity of a surface complex as the mole fraction of the surface sites that it occupies (this is relative to a standard state of complete coverage). This definition gives the correct treatment of the configurational entropy and for bidentate complexes (such as the C2 U surface complexes) this approach is essential. The surface electrostatic potential ψ_0 is defined from the surface charge distribution using the extended Stern model; we set the capacitance of the outer Helmoltz plane to 2.0 F/m^2. For the protonation reactions all of the charge is put on the 0-plane. Following previous workers (e.g., Hiemstra and Van Riemsdijk, 1996; Boily et al., 2001) we assign a charge of −0.5 to surface FeOH and Fe_3O surface groups based on Pauling's second rule. However, it has been well established (e.g., Hiemstra and Van Riemsdijk, 1996; Boily et al., 2001) that potentiometric titrations cannot resolve the FeOH and Fe_3O sites; consequently, following previous authors we will model the surface protonation of goethite using a 1-site 1-pK formalism with $\mathrm{p}K_{a1} = \mathrm{p}K_{a2} = \mathrm{p}K_{pzc}$ where $\mathrm{p}K_{pzc}$ is the pH at the point of zero charge. We fit K_a for different values of the inner-layer capacitance C_1 and the Na^+ and NO_3^- sorption constants. Our value for $\mathrm{p}K_{pzc} = 9.18$ while our value for C_1 1.05. These are close to those of Boily et al. (2001) but our value of the NO_3^- binding constant ($\log K_{NO_3^-}$) is smaller. However, changing $\log K_{NO_3^-}$ by 2 units has little effect on the calculated U surface complexation.

3.4.2. CO_3^{2-} surface complexation

We fit the carbonate sorption data of Villalobos and Leckie (2000) (open system $P(CO_2)$ in 0.1 M $NaNO_3$) to the surface complexation equilibria

$$2> \mathrm{FeOH}^{-1/2} + \mathrm{H_2CO_3} = (> \mathrm{FeO})_2\mathrm{CO}^{-1} + 2\mathrm{H_2O} \quad (2a)$$

$$> \mathrm{FeOH}^{-1/2} + \mathrm{H_2CO_3} + \mathrm{Na}+ = > \mathrm{FeOCO_2}^{-1.5}\ldots\mathrm{Na}^+ + \mathrm{H_2O} + \mathrm{H}^+ \quad (2b)$$

where the bidentate complex is dominant up to pH 9. Our model is similar to that of Hiemstra et al. (2004) but we partition the change in charge between the inner and outer of the $(>FeO)_2CO^{-1}$ complex to be +1 in the inner Helmoltz plane and −1 in the outer Helmholtz plane in the extended Stern model. The log K for reaction (2a) is 5.93 while that for reaction (2b) is −3.02.

3.4.3. U surface complexation model

As an initial attempt to model the sorption edges, we will neglect the E2 complex and assume that UO_2^{2+} only forms complexes with the $>FeOH^{-0.5}$ surface sites on the {101} surface. We assume that the $>Fe_3O^{-0.5}$ surface sites on {101} do not form complexes with UO_2^{2+}.

The formation of the C2 complex on the {101} surfaces is:

$$2(> \mathrm{FeOH}^{-1/2}) + \mathrm{UO_2}^{2+} = (> \mathrm{FeOH})_2\mathrm{UO_2}^+ \quad (3a)$$

with conditional ($I = 0.1$) equilibrium constant:

$$K_{C2} = \frac{X_{C2}\exp(-2\psi_0 F/RT)}{(X_{\mathrm{FeOH},\{101\}})^2[\mathrm{UO_2}^{2+}]} \quad (3b)$$

where X_{C2} is the mole fraction of {101} surface FeOH sites occupied by the $(> \mathrm{FeOH})_2\mathrm{UO_2}\ (\mathrm{OH})_n^{1-n}$ complex. We assign all of the UO_2^{2+} charge to the 0-plane.

The one-site surface complexation model fits to the U-goethite adsorption data are shown on Fig. 5 and summarised in Table 4. The sorption edges obtained in the absence of CO_2 (<1 ppm CO_2) at pH < 7 can be modelled using only the C2$(> \mathrm{FeOH})_2\ \mathrm{UO_2}^+$ complexes. At high surface loadings (2.6 wt% U) the sorption capacity due to simple C2 $(>FeOH)_2UO_2$ complexes is exceeded and a small fraction of polynuclear complexes are needed to model the sorption edge. Invoking a monodentate complex was unsuccessful. This may be simply an artifact of underestimating the number of surface sites available based on the {101} >FeOH site density and the BET surface area. Given the weak scattering by next-nearest-neighbor U atoms (as in metaschoepite, Fig. 5), the EXAFS spectra are not inconsistent with the presence of a small fraction of polynuclear complexes, although at pH 8 the modelled fraction of the dimer is negligible.

For sorption edges taken at $P(CO_2) = 10^{-3.5}$ bar, there is complete desorption above pH 8 due to the formation of strong UO_2CO_2 complexes in solution. This was observed by Hsi and Langmuir (1985) for goethite and Waite et al. (1994) for ferrihydrite. We find that the desorption edge cannot be modelled using only the solution species (Table 1) and the $(> \mathrm{FeOH})_2\ \mathrm{UO_2}^+$ surface complex; a $(> \mathrm{FeOH})_2\mathrm{UO_2}\ \mathrm{CO_3}^-$ complex is needed account for sorption of UO_2 at pH > 7. This complex is consistent with EXAFS spectra at pH 8 which show a U–C distance near 2.9 Å. Significantly, this complex is also significant at pH 5.5 and suggests that the 2.9 Å peak in the EXAFS may also result from U to C scattering even though the expected

Table 4
Stability constants derived from a 1-site model assuming only complexes on the {110} surface

K: Complex	ΔZ_0	ΔZ_1	log K		
			2.6 wt%	0.26 wt%	0.026 wt%
K(C2)(> FeOH)$_2UO_2^+$	2	0	13.45	13.45	14.11
K(T1) (>FeOH)$_2UO_2CO_3$	2	−2	5.20	4.37	4.35
K(T2):>FeOCO$_2UO_2$	−1	2	—	5.78	6.24
(>FeOH)$_2$(UO$_2$)$_2$(OH)$_2$	2	0	8.38	—	—
χ^2			1.5	1.6	1.0

Complexes not indicated did not comprise a significant fraction of the sorbed U. χ^2 is calculated assuming each data point has a 3% relative error.

CO_3^{2-} oxygen at 4.3 Å is not resolved. The (> FeOH)$_2$ $UO_2CO_3^-$ ternary complex is also predicted to be present at very high pH in the nominally CO_2-free experiments when the P(CO_2) in the purge gas is assumed to be 10^{-6} bar. This explains the presence of U–C scattering at pH 8 in the EXAFS of nominally CO_2-free experiments, although the U–C scattering can also be modelled by an H_2O ligand near 2.55 Å.

In addition to the effect on U sorption at pH > 7, we also find that $10^{-3.5}$ bar CO_2 enhances the sorption of UO_2^{2+} at pH < 6 relative to the P(CO_2) < 10^{-6} bar experiments. We cannot model this as an electrostatic effect due to sorbed CO_3^{2-}. Instead, we tentatively propose that there is a second ternary complex that we postulate to be (>FeO)-CO_2UO_2. Given the masking of the U–Fe scattering, the EXAFS would be unable to distinguish this complex from the (>FeOH)$_2UO_2CO_3$ complex.

For the (>FeOH)$_2UO_2CO_3$ ternary complex, we modelled the surface complexation as

$$2(> \mathrm{FeOH}^{-1/2}) + \mathrm{UO_2}^{2+} + \mathrm{H_2CO_3} = (> \mathrm{FeOH})_2\mathrm{UO_2CO_3} + 2\mathrm{H}+ \quad (4a)$$

with conditional ($I = 0.1$) equilibrium constant:

$$K_{T1} = \frac{X_{C2}[\mathrm{H}^+]^2 \exp((-2\psi_0 + 2\psi_1)F/RT)}{\left(X_{\mathrm{FeOH},\{101\}}\right)^2[\mathrm{UO_2}^{2+}][\mathrm{H_2CO_3}]} \quad (4b)$$

where X_{C2} is the mole fraction of {101} surface FeOH sites occupied by the (>FeOH)$_2UO_2CO_3$ complex. We assign the 2+ charge of the UO_2^{2+} to the 0-plane and the 2− charge of the CO_3^{2-} to the 1-plane. For the (>FeO)CO_2UO_2 we used

$$> \mathrm{FeOH}^{-1/2} + \mathrm{UO_2}^{2+} + \mathrm{H_2CO_3} = (> \mathrm{FeO})\mathrm{CO_2UO_2} + \mathrm{H}+ \quad (5a)$$

with equilibrium constant:

$$K_{T2} = \frac{X_{C2}[\mathrm{H}^+] \exp((2\psi_0 - 2\psi_1)F/RT)}{(X_{\mathrm{FeOH},\{101\}})[\mathrm{UO_2}^{2+}][\mathrm{H_2CO_3}]} \quad (5b)$$

The one-site surface complexation model is summarized in Table 4 and in Fig. 2. Note that each surface loading was fit separately but the P(CO_2) = $10^{-3.5}$ and <10^{-6} data were fit together. The stability constants are reasonably consistent as a function of surface loading although the model for 2.6 wt% loading is complicated by the presence of the inferred dimer complex. That the stability constant for the (> FeOH)$_2UO_2CO_3^-$ complex is ~0.8 log units higher at high surface loading suggest that an additional complex is present; presumably, it may involve CO_3^{2-} complexation of the suspected dimer. However, inclusion of such a complex would yield an over-determined model. The stability constant (KT2) of the proposed >FeOCO$_2UO_2$ complex is poorly constrained by the data. This complex is strongly indicated by the very large shift in the sorption edge at low pH when CO_2 is present; however, its stability constant is determined from sorption data over a very small pH range. Further experiments are needed to verify this complex and refine its stability constant.

We considered testing the importance of the E2 complex using a two-site model that would allow the E2 complex to form on the {210} surface at low surface loading. The ~12 kJ/mol energy difference between the E2 and C2 complexes derived from the *ab initio* calculations suggests that $K_{E2}/K_{C2} \sim 10^2$. (Again, this assumes that the electrostatic potentials on the {101} and {021} surfaces are the same.) Assuming the {021} surfaces comprise ~1% of the total 45 m^2/g surface area, the sorption capacity of the {021} E2 site complexes would be ~0.1 wt% U. Hence, nearly all of the UO_2^{2+} sorbed at 2.6 wt% loading (Fig. 1) must be involve only C2 complex while the UO_2^{2+} sorbed at 0.026 wt% loading must involve the E2 complex. However, because of the small energy difference between the E2 and C2 complexes, configurational entropy will favor the formation of a significant fraction of C2 complexes even at low surface loading. At intermediate loading (0.26 wt%) there should be a mixture of E2 and C2 complexes. Given that the stability constants for the main C2 complex at 0.026, 0.26 and 2.6 wt% loading are so similar, we cannot resolve an E2 site complex with the current data. We tentatively conclude that there is no evidence for E2 complexes on the {210} or {010} surfaces from the batch sorption experiments.

4. CONCLUSIONS

Based on structural considerations, we propose that the dominant surface complexation mechanism for UO_2^{2+} on goethite is by the formation of C2 complexes on the {101} surfaces. The previously proposed E2 complex can only form on the {210} or {010} surfaces which comprise only small fraction (~1%) of the goethite surface area. Consistent with this, we find that the U–Fe distance previously attributed to the E2 complex in EXAFS spectra can be fit entirely by multiple scattering. At the same time, the effect

of multiple scattering is to mask the proposed C2 complex. Although density functional calculations predict that the E2 complex is somewhat more stable than the C2 complex, surface complexation models of our sorption edges fail to resolve a second stronger complexation site. We obtain similar surface complex stability constants from surface loadings from 0.026 to 2.6 wt%.

In the presence of $10^{-3.5}$ bar CO_2, we find that nearly all surface-sorbed U occurs as the C2 ternary complex (>FeOH)UO_2CO_3. The batch sorption experiments provide evidence for an additional ternary complex (>$FeOCO_2$)UO_2 that is significant at low pH. Both complexes are consistent with EXAFS spectra if only because of the weak next-nearest neighbor scattering.

ACKNOWLEDGMENTS

Thanks are due to Bruce Patterson (University of Bristol) for assistance with ICP-MS. We are especially grateful to Bob Bilsborrow, station manager of 16.5 at the Daresbury Synchrotron radiation source, for his help in optimising the experimental conditions. Synchrotron beamtime was provided by direct access awards from CCLRC. This work was funded by NERC Grant NE/C513142/1.

APPENDIX A. SUPPLEMENTARY DATA

Supplementary data associated with this article can be found, in the online version, at doi:10.1016/j.gca.2007.10.023.

REFERENCES

Allard T., Ildefonse P., Beaucaire C. and Calas G. (1999) Structural chemistry of uranium associated with Si, Al, Fe gels in a granitic uranium mine. *Chem. Geol.* **158**, 81–103.

Allen P. G., Bucher J. J., Shuh D. K., Edelstein N. M. and Reich T. (1997) Investigation of Aquo and Chloro Complexes of UO_2^{2+}, NpO_2^+, Np^{4+}, and Pu^{3+} by X-ray Absorption Fine Structure Spectroscopy. *Inorg. Chem.* **36**, 4676–4683.

Bargar J. R., Reitmeyer R. and Davis J. A. (1999) Spectroscopic confirmation of uranium(VI)-carbonato adsorption complexes on hematite. *Environ. Sci. Technol.* **33**, 2481–2484.

Bargar J. R., Reitmeyer R., Lenhart J. J. and Davis J. A. (2000) Characterization of U(VI)-carbonato ternary complexes on hematite: EXAFS and electrophoretic mobility measurements. *Geochim. Cosmochim. Acta* **64**, 2737–2749.

Bevington P. and Robinson D. K. (2002) *Data Reduction and Error Analysis for the Physical Sciences*. McGraw-Hill, New York, pp. 326.

Binsted N. (1998) *SERC Daresbury Laboratory EXCURV98 Program*. Daresbury Laboratory, Warrington, UK.

Boily J.-F., Lutzenkirchen J., Balmes O., Beattie J. and Sjoberg S. (2001) Modelling proton binding at the goethite (α-FeOOH)-water interface. *Coll. Surf. A* **179**, 11–27.

Dent A. J. and Mosselmans J. F. W. (1992) *A Guide to EXBACK, EXCALIB, and EXCURV92*. Daresbury Laboratory, Warrington, UK.

Druchok M., Bryk T. and Holovko M. (2005) A molecular dynamics study of uranyl hydration. *J. Mol. Liquids* **120**, 11–14.

Duff M. C. and Amrhein C. (1996) Uranium(VI) adsorption on goethite and soil in carbonate solutions. *Soil Sci. Soc. Am. J.* **60**, 1393–1400.

Faas S., Snijders J. G., vanLenthe J. H., vanLenthe E. and Baerends E. J. (1995) The ZORA formalism applied to the Dirac–Fock equation. *Chem. Phys. Lett.* **246**, 632–640.

Farkas I., Banyai I., Szabo Z., Wahlgren U. and Grenthe I. (2000) Rates and Mechanisms of Water Exchange of UO_2^{2+}(aq) and UO_2(oxalate)$F(H_2O)_2^-$: A Variable-Temperature ^{17}O and ^{19}F NMR Study. *Inorg. Chem.* **39**, 799–805.

Finch R. J., Cooper M. A., Hawthorne F. C. and Ewing R. C. (1996) The crystal structure of schoepite, $(UO_2)_8O_2(OH)_{12}(H_2O)_{12}$. *Can. Mineral.* **34**, 1071–1088.

Grenthe I., Fuger J., Konings R. J. M., Lemire R. J., Muller A. B., Nguyen-Trung C. and Wanner H. (1992) *Chemical thermodynamics, Volume 1: Chemical Thermodynamics of Uranium*. North-Holland, Amsterdam, 714 pp.

Guillaumont R., Fanghanel T., Fuger J., Grenthe I., Neck V., Palmer D. A. and Rand M. H. (2003) *Chemical Thermodynamics Volume 5: Update on the Chemical Thermodynamics of Uranium, Neptunium, Plutonium, Americium and Technetium*. Elsevier, 970 pp.

Hay P. J., Martin R. L. and Schreckenbach G. (2000) Theoretical studies of the properties and solution chemistry of AnO_2^{+2} and AnO_2^+ Aquo Complexes for An=U, Np, and Pu. *J. Phys. Chem. A* **104**, 6259–6270.

Hayes K. F., Redden G., Ela W. and Leckie J. O. (1991) Surface complexation models: an evaluation of model parameter estimation using FITEQL and oxide mineral titration data. *J. Coll. Interf. Sci.* **142**, 448–469.

Hedin L. and Lundqvist S. (1969) Effects of electron-electron and electron-phonon interactions on the one-electron states of solids. *Solid State Phys.* **23**, 1–181.

Hiemstra T. and Van Riemsdijk W. H. (1996) A surface structural approach to ion adsorption: the charge distribution (CD) model. *J. Coll. Interf. Sci.* **179**, 488–508.

Hiemstra T., Rahnemaie R. and van Riemsdijk W. H. (2004) Surface complexation of carbonate on goethite: IR spectroscopy, structure and charge distribution. *J. Coll. Interf. Sci.* **278**, 282–290.

Hsi C.-K. D. and Langmuir D. (1985) Adsorption of uranyl onto ferric oxyhydroxides: applications of a surface complexation site binding model. *Geochim. Cosmochim. Acta* **49**, 2423–2432.

Klamt A. and Schuurmann G. (1993) COSMO—a new approach to dielectric screening in solvents with explicit expressions for the screening energy and its gradient. *J. Chem. Soc. Perkin Trans.* **2**, 799–805.

Klamt A. (1995) Conductor-like screening model for real solvents—a new approach to the quantitative calculation of solvation phenomena. *J. Phys. Chem.* **99**, 2224–2235.

Klamt A. and Jonas V. (1996) Treatment of the outlying charge in continuum solvation models. *J. Chem. Phys.* **105**, 9972–9981.

Klamt A., Jonas V., Burger T. and Lohrenz J. (1998) Refinement and parametrization of COSMO-RS. *J. Phys. Chem. A* **102**, 5074–5086.

Majumdar D., Roszak S., Balasubramanian K. and Nitsche H. (2003) Theoretical study of aqueous uranyl carbonate (UO_2CO_3) and its hydrated complexes: $UO_2CO_3{\cdot}nH_2O$ ($n = 1$–3). *Chem. Phys. Lett.* **372**, 232–241.

Missana T., Garcia-Gutierrez M. and Maffiotte C. (2003) Experimental and modelling study of the uranium (VI) sorption on goethite. *J. Coll. Interf. Sci.* **260**, 291–301.

Morel F. and Morgan J. (1972) Numerical method for computing equilibria in aqueous chemical systems. *Environ. Sci. Technol.* **6**, 58.

Moskaleva L. V., Krüger S., Spörl A. and Rösch N. (2004) Role of solvation in the reduction of the uranyl dication by water: a density functional study. *Inorg. Chem.* **43**, 4080–4090.

Moyes L. N., Parkman R. H., Charnock J. M., Vaughan D. J., Livens F. R., Hughes C. R. and Braithwaite A. (2000) Uranium uptake from aqueous solution by interaction with goethite, lepidocrocite, muscovite and mackinawite: and X-ray absorption spectroscopy study. *Environ. Sci. Technol.* **34**, 1062–1068.

Murakami T., Ohnuki T., Isobe H. and Sato T. (1997) Mobility of uranium during weathering. *Am. Mineral.* **82**, 888–899.

Payne T. E., Davis J. A. and Waite T. D. (1994) Uranium retention by weathered schists—the role of iron minerals. *Radiochim. Acta* **66**, 297–303.

Peacock C. L. and Sherman D. M. (2004a) Vanadium(V) adsorption onto goethite (α- FeOOH) at pH 1.5–12: a surface complexation model based on ab initio molecular geometries and EXAFS spectroscopy. *Geochim. Cosmochim. Acta* **68**, 1723–1733.

Peacock C. L. and Sherman D. M. (2004b) Copper(II) sorption onto goethite, hematite and lepidocrocite: a surface complexation model based on ab initio molecular geometries and EXAFS spectroscopy. *Geochim. Cosmochim. Acta* **68**, 2623–22637.

Perdew J. P., Chevary J. A., Vosko S. H., Jackson K. A., Pederson M. R., Singh D. J. and Fiolhais C. (1992) Atoms, molecules, solids, and surfaces—applications of the generalised gradient approximation for exchange and correlation. *Phys. Rev. B* **46**, 6671–6687.

Perdew J. P., Burke K. and Ernzerhof M. (1996) Generalized gradient approximation made simple. *Phys. Rev. Lett.* **77**, 3865–3868.

Prikryl J. D., Pickett D. A., Murphy W. M. and Pearcy E. C. (1997) Migration behaviour of naturally occurring radionuclides at the Nopal I uranium deposit, Chihuahua, Mexico. *J. Contam. Hydrol.* **26**, 61–69.

Randall S. R., Sherman D. M., Ragnarsdottir K. V. and Collins C. R. (1999) The mechanism of cadmium surface complexation on iron oxyhydroxide minerals. *Geochim. Cosmochim. Acta* **63**, 2971–2987.

Read D. (1992) Geochemical modelling of uranium redistribution in the Osamu Utsumi mine, Pocos-de-Caldas. *J. Geochem. Explor.* **45**, 503–520.

Reich T., Moll H., Arnold T., Denecke M. A., Herring C., Geipel G., Bernhard G., Nitsch H., Allen P. G., Bucher J. J., Edelstein N. M. and Shuh D. K. (1998) An EXAFS study of uranium(VI) sorption onto silica gel and ferrihydrite. *J. Electron Spect. Rel. Phenom.* **96**, 237–243.

Schwertmann U. and Cornell R. M. (1991) *Iron Oxides in the Laboratory: Preparation and Characterization*. VCH Publishers.

Schwertmann U. and Murad E. (1983) Effect of pH on the formation of goethite and hematite from ferrihydrite. *Clays Clay Miner.* **31**, 277–284.

Steele H. M., Wright K. and Hillier I. H. (2002) Modelling the adsorption of uranyl on the surface of goethite. *Geochim. Cosmochim. Acta* **66**, 1305–1310.

te Velde G., Bickelhaupt F. M., Baerends E. J., Fonseca Guerra C., van Gisbergen S. J. A., Snijders J. G. and Ziegler T. (2001) Chemistry with ADF. *J. Comput. Chem.* **22**, 931–967.

Thompson H. A., Brown G. E. and Parks G. A. (1997) XAFS spectroscopic study of uranyl coordination in solids and aqueous solution. *Am. Mineral.* **82**, 483–496.

Ulrich K.-U., Rossberg A., Foerstendorfa H., Zänkera H. and Scheinost A. C. (2006) Molecular characterization of uranium(VI) sorption complexes on iron(III)-rich acid mine water colloids. *Geochim. Cosmochim. Acta* **70**, 5469–5487.

Villalobos M. and Leckie J. O. (2000) Carbonate adsorption on goethite under closed and open CO_2 conditions. *Geochim. Cosmochim. Acta* **64**, 3787–3802.

von Gunten H. R., Roessler E., Lowson R. T., Reid R. D. and Short S. A. (1999) Distribution of uranium- and thorium series radionuclides in mineral phases of a weathered lateritic transect of a uranium ore body. *Chem. Geol.* **160**, 225–240.

Waber N., Schorscher H. D. and Peters T. (1992) Hydrothermal and supergene uranium mineralization at the Osamu Utsumi mine, Pocos-de-caldas, Minas-Gerais, Brazil. *J. Geochem. Explor.* **45**, 53–112.

Waite T. D., Davis J. A., Payne T. E., Waychunas G. A. and Xu N. (1994) Uranium(VI) adsorption to ferrihydrite—application of a surface complexation model. *Geochim. Cosmochim. Acta* **58**, 5465–5478.

Associate editor: James R. Rustad